Predictive Active Steering Control for Autonomous Vehicle Systems

Paolo Falcone, Francesco Borrelli, Jahan Asgari, Hongtei Eric Tseng, and Davor Hrovat, *Fellow, IEEE*

Abstract—In this paper, a model predictive control (MPC) approach for controlling an active front steering system in an autonomous vehicle is presented. At each time step, a trajectory is assumed to be known over a finite horizon, and an MPC controller computes the front steering angle in order to follow the trajectory on slippery roads at the highest possible entry speed. We present two approaches with different computational complexities. In the first approach, we formulate the MPC problem by using a nonlinear vehicle model. The second approach is based on successive online linearization of the vehicle model. Discussions on computational complexity and performance of the two schemes are presented. The effectiveness of the proposed MPC formulation is demonstrated by simulation and experimental tests up to 21 m/s on icy roads.

Index Terms—Active steering, autonomous vehicles, model predictive control, nonlinear optimization, vehicle dynamics control, vehicle stability.

I. INTRODUCTION

RECENT trends in automotive industry point in the direction of increased content of electronics, computers, and controls with emphasis on the improved functionality and overall system robustness. While this affects all of the vehicle areas, there is a particular interest in active safety, which effectively complements the passive safety counterpart. Passive safety is primarily focused on the structural integrity of vehicle. Active safety on the other hand is primarily used to avoid accidents and at the same time facilitate better vehicle controllability and stability especially in emergency situations, such as what may occur when suddenly encountering slippery parts of the road [10].

Early works on active safety systems date back to the 1980s and were primarily focused on improving longitudinal dynamics part of motion, in particular, on more effective braking (ABS) and traction control (TC) systems. ABS systems increase the braking efficiency by avoiding the lock of the braking wheels. TC systems prevent the wheel from slipping and at the same time improves vehicle stability and steerability by maximizing the tractive and lateral forces between the vehicle's tire and the road. This was followed by work on different vehicle

stability control systems [34] (which are also known under different acronyms such as electronic stability program (ESP), vehicle stability control (VSC), interactive vehicle dynamics (IVD), and dynamic stability control (DSC)). Essentially, these systems use brakes on one side and engine torque to stabilize the vehicle in extreme limit handling situations through controlling the yaw motion.

In addition to braking and traction systems, active front steering (AFS) systems make use of the front steering command in order to improve lateral vehicle stability [1], [2]. Moreover, the steering command can be used to reject external destabilizing forces arising from μ-split, asymmetric braking, or wind [21]. Four-wheel steer (4WS) systems follow similar goals. For instance, in [3], Ackermann *et al.* present a decoupling strategy between the path following and external disturbances rejection in a four-wheel steering setup. The automatic car steering is split into the path following and the yaw stabilization tasks, the first is achieved through the front steering angle, the latter through the rear steering angle.

Research on the AFS systems has also been approached from an autonomous vehicle perspective. In [16], an automatic steering control for highway automation is presented, where the vehicle is equipped with magnetic sensors placed on the front and rear bumpers in order to detect a lane reference implemented with electric wire [13] and magnetic markers [36]. A more recent example of AFS applications in autonomous vehicles is the "Grand Challenge" race driving [5], [23], [30].

In this paper, it is anticipated that the future systems will be able to increase the effectiveness of active safety interventions beyond what is currently available. This will be facilitated not only by additional actuator types such as 4WS, active steering, active suspensions, or active differentials, but also by additional sensor information, such as onboard cameras, as well as infrared and other sensor alternatives. All these will be further complemented by global positioning system (GPS) information including prestored mapping. In this context, it is possible to imagine that future vehicles would be able to identify obstacles on the road such as an animal, a rock, or fallen tree/branch, and assist the driver by following the best possible path, in terms of avoiding the obstacle and at the same time keeping the vehicle on the road at a safe distance from incoming traffic. An additional source of information can also come from surrounding vehicles and environments which may convey the information from the vehicle ahead about road condition, which can give a significant amount of preview to the controller. This is particular is useful if one travels on snow or ice covered surfaces. In this case, it is very easy to reach the limit of vehicle handling capabilities.

Anticipating sensor and infrastructure trends toward increased integration of information and control actuation agents,

it is then appropriate to ask what is the optimum way in controlling the vehicle maneuver for a given obstacle avoidance situation.

We assume that a trajectory planning system is available and we consider a double lane change scenario on a slippery road, with a vehicle equipped with a fully autonomous guidance system. In this paper, we focus on the control of the yaw and lateral vehicle dynamics via active front steering. The control input is the front steering angle and the goal is to follow the desired trajectory or target as close as possible while fulfilling various constraints reflecting vehicle physical limits and design requirements. The future desired trajectory is known only over finite horizon at each time step. This is done in the spirit of model predictive control (MPC) [14], [26] along the lines of our ongoing internal research efforts dating from early 2000 (see [7] and references therein).

In this paper, two different formulations of the AFS MPC problem will be presented and compared. The first one follows the work presented in [7] and uses a *nonlinear vehicle model* to *predict* the future evolution of the system [26]. The resulting MPC controller requires a nonlinear optimization problem to be solved at each time step. We will show that the computational burden is currently an obstacle for experimental validation at high vehicle speed. The second formulation tries to overcome this problem and presents a suboptimal MPC controller based on successive online linearization of the nonlinear vehicle model. This is linearized around the current operating point at each time step and a linear MPC controller is designed for the resulting linear time-varying (LTV) system. The idea of using time varying models goes back to the early 1970s in the process control field although it has been properly formalized only recently. Studies on linear parameter varying (LPV) MPC schemes can be found in [9], [18], [20], [22], and [35]. Among them, the work in [18] and [20] is the closest to our approach and it presents an MPC scheme for scheduled LTV models which has been successfully validated on a Boeing aircraft. In general, the performance of such a scheme is highly dependant on the nonlinearities of the model. In fact, as the state and input trajectories deviate from the current operating point, the model mismatch increases. This can generate large prediction errors with a consequent instability of the closed-loop system. We will show that, in our application, a state constraint can be introduced in order to significantly enhance the performance of the system. Experimental results show that the vehicle can be stabilized up to 21 m/s on icy roads. Finally, an LTV MPC with a one-step control horizon is presented. This can be tuned in order to provide acceptable performance and it does not require any complex optimization software.

We implemented the MPC controllers in real time on a passenger car, and performed tests on snow covered and icy roads. The last part of this paper describes the experimental setup and presents the experimental and simulation results of the proposed MPC controllers. It should be noted that our early work in [7] focuses on the vehicle dynamical model and on simulation results of the nonlinear MPC scheme only.

This paper is structured as follows. Section II describes the used vehicle dynamical model with a brief discussion on tire models. Section III introduces a simplified hierarchical
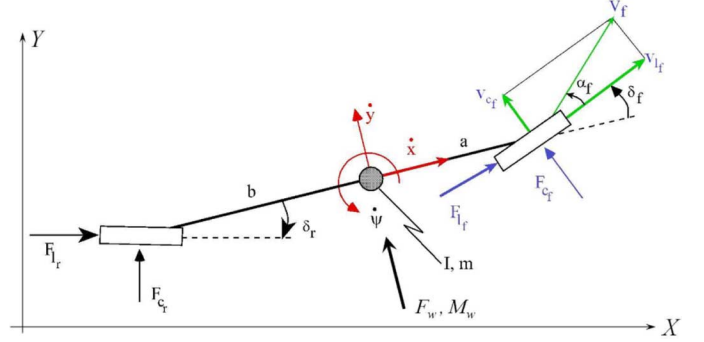

Fig. 1. Simplified vehicle "bicycle model."

framework for autonomous vehicle guidance. The contribution and the research topic of this paper are described in details and put in perspective with existing work and future research. Section IV formulates the control problem when the nonlinear and the linear prediction models are used. The double lane change scenario is described in Section V, while in Section VI, the experimental and simulation results are presented. This is then followed by concluding remarks in Section VII which highlight future research directions.

II. MODELING

This section describes the vehicle and tire model used for simulations and control design. This section has been extracted from [7] and it is included in this paper for the sake of completeness and readability. We denote by F_l and F_c the longitudinal (or "tractive") and lateral (or "cornering") tire forces, respectively, F_x and F_y are the forces in car body frame, F_z is the normal tire load, I is the car inertia, X and Y are the absolute car position inertial coordinates, a and b are the car geometry (distance of front and rear wheels from center of gravity), g is the gravitational constant, m is the car mass, r is the wheel radius, s is the slip ratio, v_l and v_c are the longitudinal and lateral wheel velocities, x and y are the local lateral and longitudinal coordinates in car body frame, $\dot{x}$ is the vehicle speed, α is the slip angle, δ is the wheel steering angle, μ is the road friction coefficient, and ψ is the heading angle. The lower subscripts $(\cdot)_f$ and $(\cdot)_r$ particularize a variable at the front wheel and the rear wheel, respectively, e.g., F_{l_f} is the front wheel longitudinal force.

A. Vehicle Model

A "bicycle model" [25] is used to model the dynamics of the car under the assumption of a constant tire normal load, i.e., F_{z_f}, $F_{z_r} = \text{constant}$. Fig. 1 depicts a diagram of the vehicle model, which has the following longitudinal, lateral, and turning or yaw degrees of freedom:

$$m\ddot{x} = m\dot{y}\dot{\psi} + 2F_{x_f} + 2F_{x_r} \tag{1a}$$

$$m\ddot{y} = -m\dot{x}\dot{\psi} + 2F_{y_f} + 2F_{y_r} \tag{1b}$$

$$I\ddot{\psi} = 2aF_{y_f} - 2bF_{y_r}. \tag{1c}$$

The vehicle's equations of motion in an absolute inertial frame are

$$\dot{X} = \dot{x}\cos\psi - \dot{y}\sin\psi, \quad \dot{Y} = \dot{x}\sin\psi + \dot{y}\cos\psi. \tag{2}$$

The wheel's equations of motion describe the lateral (or cornering) and longitudinal wheel velocities

$$v_{l_f} = v_{y_f} \sin \delta_f + v_{x_f} \cos \delta_f \qquad (3a)$$
$$v_{l_r} = v_{y_r} \sin \delta_r + v_{x_r} \cos \delta_r \qquad (3b)$$
$$v_{c_f} = v_{y_f} \cos \delta_f - v_{x_f} \sin \delta_f \qquad (3c)$$
$$v_{c_r} = v_{y_r} \cos \delta_r - v_{x_r} \sin \delta_r \qquad (3d)$$

where δ_f and δ_r are front and rear wheel steering angle, respectively, and

$$v_{y_f} = \dot{y} + a\dot{\psi}, \quad v_{y_r} = \dot{y} - b\dot{\psi} \qquad (4a)$$
$$v_{x_f} = \dot{x}, \qquad v_{x_r} = \dot{x}. \qquad (4b)$$

The following equations hold for rear and front axes by using the corresponding subscript for *all* the variables. Longitudinal and lateral tire forces lead to the following forces acting on the center of gravity:

$$F_y = F_l \sin \delta + F_c \cos \delta, \quad F_x = F_l \cos \delta - F_c \sin \delta. \qquad (5a)$$

Tire forces F_l and F_c for each tire are given by

$$F_l = f_l(\alpha, s, \mu, F_z), \quad F_c = f_c(\alpha, s, \mu, F_z) \qquad (6)$$

where α, s, μ, and F_z are defined next. The tire slip angle α represents the angle between the wheel velocity vector v_f and the direction of the wheel itself, and can be compactly expressed as

$$\alpha = \arctan \frac{v_c}{v_l}. \qquad (7)$$

The slip ratio s is defined as

$$s = \begin{cases} \frac{r\omega}{v_l} - 1, & \text{if } v_l > r\omega, v_l \neq 0 \text{ for braking} \\ 1 - \frac{v_l}{r\omega}, & \text{if } v_l < r\omega, \omega \neq 0 \text{ for driving} \end{cases} \qquad (8)$$

where r and ω are the radius and the angular speed of the wheel, respectively. The parameter μ represents the road friction coefficient and is assumed equal for front and rear wheels. F_z is the total vertical load of the vehicle and is distributed between the front and rear wheels based on the geometry of the car model (described by the parameters a and b)

$$F_{z_f} = \frac{bmg}{2(a+b)}, \quad F_{z_r} = \frac{amg}{2(a+b)}. \qquad (9)$$

The nonlinear vehicle dynamics described in (1)–(9), can be rewritten in the following compact from:

$$\frac{d\xi}{dt} = f_{s(t), \mu(t)}(\xi(t), u(t)) \qquad (10)$$

where the dependence on slip ratio s and friction coefficient value μ at each time instant has been explicitly highlighted. The state and input vectors are $\xi = [\dot{y}, \dot{x}, \psi, \dot{\psi}, Y, X]'$ and $u = \delta_f$, respectively. In this paper, δ_r is assumed to be zero at any time instant.

Model (10) captures the most relevant nonlinearities associated to lateral stabilization of the vehicle. Section II-B briefly describes the models of tire forces F_l and F_c.
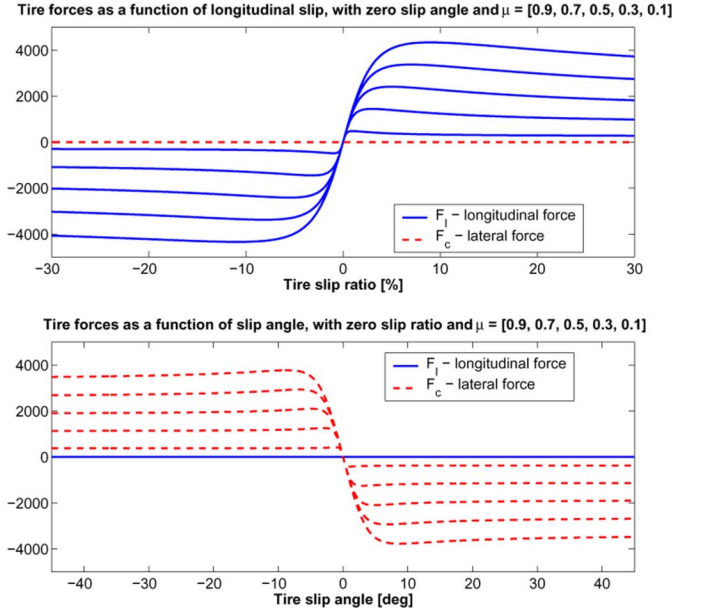

Fig. 2.   Longitudinal and lateral tire forces with different μ coefficient values.

B. Tire Model

With the exception of aerodynamic forces and gravity, all of the forces which affect vehicle handling are produced by the tires. Tire forces provide the primary external influence and, because of their highly nonlinear behavior, cause the largest variation in vehicle handling properties throughout the longitudinal and lateral maneuvering range. Therefore, it is important to use a realistic nonlinear tire model, especially when investigating large control inputs that result in response near the limits of the maneuvering capability of the vehicle. In such situations, the lateral and longitudinal motions of the vehicle are strongly coupled through the tire forces, and large values of slip ratio and slip angle can occur simultaneously.

Most of the existing tire models are predominantly "semi-empirical" in nature. That is, the tire model structure is determined through analytical considerations, and key parameters depend on tire data measurements. Those models range from extremely simple (where lateral forces are computed as a function of slip angle, based on one measured slope at $\alpha = 0$ and one measured value of the maximum lateral force) to relatively complex algorithms, which use tire data measured at many different loads and slip angles.

In this paper, we use a Pacejka tire model [4] to describe the tire longitudinal and cornering forces in (6). This is a complex, semi-empirical nonlinear model that takes into consideration the interaction between the longitudinal force and the cornering force in combined braking and steering. The longitudinal and cornering forces are assumed to depend on the normal force, slip angle, surface friction coefficient, and longitudinal slip. Fig. 2 depicts longitudinal and lateral forces versus longitudinal slip and slip angle, for fixed values of the friction coefficients. We remark that the front tire of the "bicycle" model represents the two front tires of the actual car.
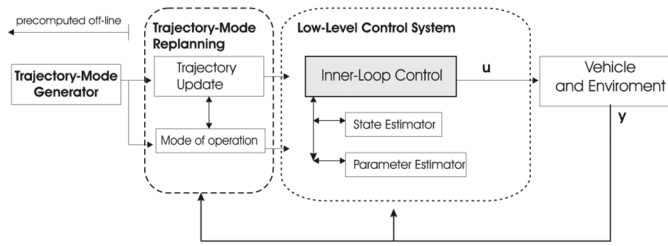
Fig. 3. Simplified architecture for fully autonomous vehicle guidance system.

III. HIERARCHICAL FRAMEWORK FOR AUTONOMOUS GUIDANCE

In this section, we borrow the simplified schematic architecture in Fig. 3 from the aerospace field [8], [24], [31], in order to explain our approach and contribution. The architecture in Fig. 3 describes the main elements of an autonomous vehicle guidance system and it is composed of four modules: the trajectory/mode generator, the trajectory/mode replanning, the low-level control system, and the vehicle and the environmental model. The trajectory/mode planning module precomputes offline the vehicle trajectory together with the timing and conditions for operation mode change. In the aerospace field, examples of operation mode selection include aeroshell parachute deployment or heatshield release, in the automotive field this could include switching between two or more types of energy sources (i.e., gas, electricity, hydrogen) or (in a very futuristic scenario) morphing between different vehicle shapes.

The trajectory and the mode of operation computed offline can be recomputed online during the drive by the trajectory/mode replanning module based on current measurements, at fixed points or on the occurrence of certain events (such as tracking errors exceeding certain bounds, hardware failure, excessive wind, the presence of a pop-up obstacle).

The low-level control system commands the vehicle actuators such as front and rear steering angles, four brakes, engine torque, active differential, and active suspensions based on sensor measurements, states, and parameters estimations and reference commands coming from the trajectory/mode replanning module. Such reference commands can include lateral and longitudinal positions, pitch, yaw, and roll rates. The low-level control system objective is to keep the vehicle as close as possible to the currently planned trajectory despite measurement noise, unmodeled dynamics, parameteric uncertainties, and sudden changes on vehicle and road conditions which are not (or not yet) taken into account by the trajectory replanner. In particular, when a vehicle is operating near its stability limit, these additional noises, disturbances, and uncertainties must be considered, possibly through detecting the vehicle's internal state, and compensated for. For example, if rear tires saturate, a skillful driver would switch his/her steering input from the usual steering command for trajectory following to a counter-steering one for stabilizing the vehicle. It is conceivable that an automated steering would not produce the necessary stabilizing counter-steer if the commanded steering is only a function of the desired trajectory and vehicle's current position and heading (without considering additional vehicle dynamic states).

We remark that the scheme in Fig. 3 is an oversimplified scheme and that additional hierarchical levels could be present both in the trajectory/mode replanning module and in the low-level control system module. The union of the first three modules is often referred to as guidance and navigation control (GNC) system.

Typically, the trajectory replanner and the low-level control system modules do not share the same information on environment and vehicle. For instance, the replanning algorithms can use information coming from cameras or radars which may not be used at the lower level. Also, typically, the frequency at which the trajectory replanning module is executed is lower than the one of the lower level control system. The design of both modules makes use of vehicle and environment models with different levels of detail. The fidelity of the dynamical model used for the design of the two modules is dictated, among many factors, by a performance/computational resource compromise and, in the literature, there is no accepted standard on this. One of the possible control paradigms for the two modules consists in using a high-fidelity vehicle model for designing the lower level controller while the trajectory planner relies on a rougher/less detailed dynamical model of the vehicle. Clearly, the higher the fidelity of the models used at the higher level is, the easier the job for the lower level control algorithm becomes.

Studies on GNC algorithms vary in 1) the focus (trajectory replanner and/or the low-level control system); 2) the type of vehicle dynamical model used; 3) the type of control design used; and 4) inputs and sensors choice.

In [23], the trajectory replanner module is based on a receding horizon control design. The planning problem is formulated as a constrained optimization problem minimizing a weighted sum of arrival time, steering, and acceleration control efforts. The vehicle model is a simple rear-centered kinematic model with acceleration, speed, steering, steering rate, and rollover constraints. The lower level control module uses two separated proportional–integral–differentials (PIDs) to control longitudinal and lateral dynamics. The longitudinal controller acts on throttle and brakes while the lateral controls on the steering angle.

The GNC architecture in [30] is similar to [23]. The trajectory planning task is posed as a constrained optimization problem. The cost function penalizes obstacles collision, distance from the precomputed offline trajectory and the lateral offset from the current trajectory. At the lower level, a PI controller acts on brakes and throttle to control the longitudinal dynamics. A simple nonlinear controller, instead, is used to control the lateral dynamics through the steering angle. Details on the vehicle dynamical model used in [30] are not disclosed. In [29], a scheme similar to the one in [23] is used to design a GNC systems for a flight control application.

In [33], an explicit MPC scheme has been applied at the lower level control to allocate four wheel slips in order to get a desired yaw moment. The steering angle is not controlled.

In this paper, we assume that the path can be generated with two different methods. In the first, the trajectory is established by simply driving a test vehicle slowly along the desired path, e.g., a double lane change manoeuvre. The actual path is recorded by differential GPS and then used as a desired path for subsequent tests at higher speed. This method has been used

in [34] to generate the reference path for a steering robot on high μ. In this case, no trajectory replanning is needed and the contribution of the work presented in this paper is to facilitate systematic and repeatable tests of safety critical emergency manoeuvres during limit conditions, such as obstacle avoidance manoeuvres on slippery surfaces, i.e., snow and ice. In the second method, we assume that a trajectory replanning module is available and the trajectory is recomputed at a less frequent rate than the frequency of the lower level controller. For both cases, we focus on the lower level control design by means of nonlinear and LTV MPC for the specific scenario of an active steering system.

As suggested in [28], there is a significant challenge involved in obtaining the steering required to accomplish the limit maneuver considered in this paper while maintaining vehicle stability. By focusing on the lower level MPC controller, we also believe that the resultant steering may mimic a skillful driver who takes the full vehicle dynamic states into account. *Compared to the lower level control algorithms* presented in the aforementioned literature, our approach 1) is model based and uses the vehicle model (10) and the highly nonlinear Pacejka tire model described in Section II-B; 2) includes constraints on inputs and states in the control design; 3) is systematic and multivariable and can accommodate new actuators and higher fidelity models. Moreover, we have experimentally validated the controller presented in this paper with a dSPACE AutoBox system which is a standard rapid prototyping system used in automotive industries [11].

IV. ACTIVE STEERING CONTROLLER DESIGN

In this section, we introduce the control design procedure for the proposed path following problem via an active steering system.

Desired references for the heading angle ψ, the yaw rate $\dot{\psi}$, and the lateral distance Y define a desired path over a finite horizon. The nonlinear vehicle dynamics (10) and the Pacejka tire model are used to predict the vehicles behavior, and the front steering angle δ_f is chosen as control input. The rear steering angle is assumed to be zero $\delta_r = 0$, the tire slip ratios s_f and s_r are measured, and the road friction μ is estimated at each time instant. The approach used in [6] can be used for the online estimation of μ.

A MPC scheme is used to solve the path following problem. The main concept of MPC is to use a *model* of the plant to *predict* the future evolution of the system [6], [14], [17], [26], [27]. At each sampling time, starting at the current state of the vehicle, an open-loop optimal control problem is solved over a finite horizon. The open-loop optimal control problem minimizes the deviations of the predicted outputs from their references over a sequence of future steering angles, subject to operating constraints. The resulting optimal command signal is applied to the process only during the following sampling interval. At the next time step, a new optimal control problem based on new measurements of the state is solved over a shifted horizon.

In the following two different formulations of the AFS MPC problem will be presented. Section IV-A describes the first MPC formulation as presented in the preliminary work [7]. There, the

nonlinear vehicle model (10) and the Pacejka tire model are used to predict the future evolution of the system. The minimization of a quadratic performance index, subject to the nonlinear vehicle dynamics, is a nonlinear optimization problem. Such optimization problem is solved online, at each time step. This can be computationally demanding, depending on the vehicles states and constraints. The second formulation, presented in Section IV-B, tries to overcome this problem. A LTV approximation of vehicle model (10) and the Pacejka tire model are used to predict the future evolution of the system. This leads to a suboptimal LTV MPC controller. In this case, a time varying convex quadratic optimization problem is formulated and solved at each time step, leading to the reduction of the computational burden with an acceptable loss of performance. We will show that the MPC performance is enhanced by including a constraint on the tire slip angle which stabilizes the vehicle at high speed.

A. Nonlinear (NL) MPC

In order to obtain a finite-dimensional optimal control problem, we discretize the system dynamics (10) with a fixed sampling time T_s

$$\xi(k+1) = f_{s(k),\mu(k)}^{dt}(\xi(k), \Delta u(k)) \tag{11a}$$
$$u(k) = u(k-1) + \Delta u(k) \tag{11b}$$

where the Δu formulation is used, with $u(k) = \delta_f(k)$ and $\Delta u(k) = \Delta\delta_f(k)$.

We define the following output map for yaw angle and lateral position states:

$$\eta(k) = h(\xi(k)) = \begin{bmatrix} 0 & 0 & 1 & 0 & 0 & 0 \\ 0 & 0 & 0 & 0 & 1 & 0 \end{bmatrix} \xi(k) \tag{12}$$

and consider the following cost function:

$$J(\xi(t), \Delta\mathcal{U}_t) = \sum_{i=1}^{H_p} \left\| \eta_{t+i,t} - \eta_{\text{ref}\,t+i,t} \right\|_Q^2 + \sum_{i=0}^{H_c-1} \left\| \Delta u_{t+i,t} \right\|_R^2 \tag{13}$$

where $\eta = [\psi, Y]$ and η_{ref} denote the corresponding reference signal. At each time step t, the following finite horizon optimal control problem is solved:

$$\min_{\Delta\mathcal{U}_t} \quad J(\xi_t, \Delta\mathcal{U}_t) \tag{14a}$$
$$\text{subj. to} \quad \xi_{k+1,t} = f_{s_{k,t},\mu_{k,t}}^{dt}(\xi_{k,t}, \Delta u_{k,t}) \tag{14b}$$
$$\eta_{k,t} = h(\xi_{k,t}) \tag{14c}$$
$$\mu_{k,t} = \mu_{t,t}, \quad s_{k,t} = s_{t,t} \tag{14d}$$
$$k = t, \ldots, t + H_p$$
$$\delta_{f,\min} \le u_{k,t} \le \delta_{f,\max} \tag{14e}$$
$$\Delta\delta_{f,\min} \le \Delta u_{k,t} \le \Delta\delta_{f,\max} \tag{14f}$$
$$u_{k,t} = u_{k-1,t} + \Delta u_{k,t} \tag{14g}$$
$$k = t, \ldots, t + H_c - 1$$
$$\Delta u_{k,t} = 0, \quad k = t + H_c, \ldots, t + H_p \tag{14h}$$
$$\xi_{t,t} = \xi(t) \tag{14i}$$

where $\Delta \mathcal{U}_t = [\Delta u_{t,t}, \ldots, \Delta u_{t+H_c-1,t}]$ is the optimization vector at time t, $\eta_{t+i,t}$ denotes the output vector predicted at time $t + i$ obtained by starting from the state $\xi_{t,t} = \xi(t)$, and applying to system (11) and (12) the input sequence $\Delta u_{t,t}, \ldots, \Delta u_{t+i,t}$. H_p and H_c denote the output prediction horizon and the control horizon, respectively. We use $H_p > H_c$ and the control signal is assumed constant for all $H_c \leq t \leq H_p$. We assume slip and friction coefficient values constant and equal to the estimated values at time t over the prediction horizon [constraint (14d)].

In (13), the first summand reflects the penalty on trajectory tracking error while the second summand is a measure of the steering effort. Q and R are weighting matrices of appropriate dimensions.

We denote by $\Delta \mathcal{U}_t^* \triangleq [\Delta u_{t,t}^*, \ldots, \Delta u_{t+H_c-1,t}^*]'$ the sequence of optimal input increments computed at time t by solving (14) for the current observed states $\xi(t)$. Then, the first sample of $\Delta \mathcal{U}_t^*$ is used to compute the optimal control action and the resulting state feedback control law is

$$u(t, \xi(t)) = u(t-1) + \Delta u_{t,t}^*(t, \xi(t)). \quad (15)$$

At the next time step $t + 1$, the optimization problem (14) is solved over a shifted horizon based on the new measurements of the state $\xi(t+1)$.

B. LTV MPC

Let t be the current time and $\xi(t)$ and $u(t-1)$ be the current state and the previous input of system (11) and (12), respectively. We consider the following optimization problem:

$$\min_{\Delta \mathcal{U}_t, \epsilon} \quad \sum_{i=1}^{H_p} \left\| \delta \eta_{t+i,t} - \delta \eta_{\mathrm{ref}\, t+i,t} \right\|_Q^2$$
$$+ \sum_{i=0}^{H_c-1} \left\| \delta u_{t+i,t} \right\|_R^2 + \rho \epsilon \quad (16a)$$

$$\text{subj. to} \quad \delta \xi_{k+1,t} = \mathcal{A}_t \delta \xi_{k,t} + \mathcal{B}_t \delta u_{k,t} \quad (16b)$$

$$\delta \alpha_{k,t} = \mathcal{C}_t \delta \xi_{k,t} + \mathcal{D}_t \delta u_{k,t} \quad (16c)$$

$$\delta \eta_{k,t} = \begin{bmatrix} 0 & 0 & 1 & 0 & 0 & 0 \\ 0 & 0 & 0 & 1 & 0 & 0 \\ 0 & 0 & 0 & 0 & 1 & 0 \end{bmatrix} \delta \xi_{k,t} \quad (16d)$$
$$k = t, \ldots, t + H_p$$

$$u_{k,t} = u(t-1) + \delta u_{k,t} \quad (16e)$$

$$u_{t-1,t} = u(t-1) \quad (16f)$$

$$\Delta u_{k,t} = u_{k,t} - u_{k-1,t} \quad (16g)$$

$$\delta_{f,\min} \leq u_{k,t} \leq \delta_{f,\max} \quad (16h)$$

$$\Delta \delta_{f,\min} \leq \Delta u_{k,t} \leq \Delta \delta_{f,\max} \quad (16i)$$
$$k = t, \ldots, t + H_c - 1$$

$$\delta \alpha_{\min} - \epsilon \leq \delta \alpha_{k,t} \leq \delta \alpha_{\max} + \epsilon, \quad (16j)$$
$$k = t, \ldots, t + H_p$$

$$\Delta u_{k,t} = 0, \quad k = t + H_c, \ldots, t + H_p \quad (16k)$$

$$\epsilon \geq 0 \quad (16l)$$

$$\delta \xi_{t,t} = 0 \quad (16m)$$

where $\Delta \mathcal{U}_t \triangleq [\delta u_{t,t}, \ldots, \delta u_{t+H_c-1,t}]'$ and model (16b) and (16c) is obtained by linearizing model (11) at each time step t around the point $\xi(t)$, $u(t-1)$, for the estimated $s(t)$, $\mu(t)$. The variables $\delta \eta = [\delta \psi, \delta \dot{\psi}, \delta Y]$ and $\delta \eta_{\mathrm{ref}}$ denote the outputs of the linearized system and the corresponding reference signal, respectively. The variable $\delta \alpha$ denotes the tire slip angle variation and it is an additional output of the linearized model which is only constrained and not tracked. Inequalities (16j) are soft constraints on the tire slip angle and ϵ is a slack variable. The term $\rho \epsilon$ in (16b) penalizes the violation of the constraint on the slip angle and ρ is a weight coefficient.

The optimization problem (16) can be recast as a quadratic program (QP) (details can be found in [7]). We denote by $\Delta \mathcal{U}_t^* \triangleq [\delta u_{t,t}^*, \ldots, \delta u_{t+H_c-1,t}^*]'$ the sequence of optimal input deviations computed at time t by solving (16) for the current observed states $\xi(t)$. Then, the first sample of $\Delta \mathcal{U}_t^*$ is used to compute the optimal control action and the resulting state feedback control law is

$$u(t, \xi(t)) = u(t-1) + \delta u_{t,t}^*(t, \xi(t)). \quad (17)$$

At the next time step $t + 1$ the optimization problem (16) is solved over a shifted horizon based on the new measurements of the state $\xi(t+1)$ and based on an updated linear model (16b)–(16d) computed by linearizing the nonlinear vehicle model (11) around the new state, slip ratio, road friction coefficient, and previous input.

We remark that model (11) is linearized around an operating point that, in general, is not an equilibrium point. Therefore, the linear time-invariant (LTI) model (16b)–(16d) at time t is used to predict the state and the output deviations from the trajectories $\hat{\xi}_t(k)$, $\hat{\alpha}_t(k)$, $\hat{\eta}_t(k)$ for $k = t, \ldots, t + H_p$, respectively, computed by solving (11) with $\xi(t)$ as initial condition and $u(k) = u(t-1)$ for $k = t, \ldots, t+H_p$. Accordingly, the optimization variables $[\delta u_{t,t}, \ldots, \delta u_{t+H_c-1,t}]$ represent the input variation with respect to the previous input $u(t-1)$.

Alternatively, the vehicle model (11) can be linearized around a nominal input $u_{\mathrm{nom}}(k)$ and state trajectory $\xi_{\mathrm{nom}}(k)$. In this case, (16e) would become $u_{k,t} = u_{\mathrm{nom}}(k) + \delta u_{k,t}$ and the optimization variables $[\delta u_{t,t}, \ldots, \delta u_{t+H_c-1,t}]$ would represent the input variations around the nominal input. This approach requires a nominal input and state trajectory, i.e., $u_{\mathrm{nom}}(k)$ and $\xi_{\mathrm{nom}}(k)$. Such trajectory could be computed from the higher level replanning algorithm described in Section III or from the lower level MPC controller. We remark that in this case an LTV model over the prediction horizon $(\mathcal{A}_{t,k}, \mathcal{B}_{t,k}, \mathcal{C}_{t,k}, \mathcal{D}_{t,k})$, $k = t, \ldots, t + H_p - 1$ could be used at each time step t instead of the LTI model (16b)–(16d).

An MPC scheme similar to the one presented in this paper can be found in [18], [19], and [20]. In these works, a similar MPC formulation is used. An LTI prediction model is used to predict the behavior of the system over the prediction horizon. The LTI model is updated according to the values of flight condition dependent scheduling parameters. In [19] and [20], the LTI model is obtained by interpolation over a precomputed database of linearized models, while in [18] the LTI model is obtained by linearizing the nonlinear kinematics around the current measurements.

When evaluating the online computational burden of the proposed scheme, in addition to the time required to solve the optimization problem (16), one needs to consider the resources spent in computing the linear models $(\mathcal{A}_t, \mathcal{B}_t, \mathcal{C}_t, \mathcal{D}_t)$ in (16b) and (c) and translating (16) into a standard quadratic programming (QP) problem. Nevertheless, for the proposed application, complexity of the MPC (16) and (17) greatly reduces compared to the NL MPC presented in Section IV-A. This will be shown for a specific scenario in Sections VI-A and VI-B.

The stability of the presented control scheme is difficult to prove even under no model mismatch and it is a topic of current research. Also, robustness of nonlinear MPC schemes is an active area of research by itself. An analytical and meaningful study of the robustness of the proposed scheme would be even more difficult. The uncertainty of the tire characteristics and the road condition are often difficult to describe with a mathematical formalism which is realistic and not too conservative.

It should be noted that in the MPC scheme (16) and (17), the introduction of the state constraints (16j) is needed in order to obtain an acceptable performance and it is a contribution of this paper. As shown next in Section VI-A, such constraint arises from a careful study of the closed-loop behavior of the nonlinear MPC presented in Section IV-A. In fact, extensive simulations have shown that the nonlinear MPC never exceeds certain tire slip angles under stable operations. By removing the constraints (16j) the performance of the LTV MPC controller (16) and (17) is not acceptable and the system becomes unstable at high vehicle speeds. In fact, a simple linear model is not able to predict the change of slope in the tires characteristic (see Fig. 2). To overcome this issue, we included constraints (16j) in the optimization problem, in order to forbid the system from entering a strongly nonlinear and possibly unstable region of the tire characteristic. In particular, by looking at the tire characteristics in Fig. 2, it is clear that a linear approximation of the tire model around the origin is no longer valid if the slip angle exceeds certain bounds. Led by this observation and by a study on the closed-loop behavior of the nonlinear MPC presented in Section IV-A, we included the constraints (16j) in the optimization problem. In particular, for a given μ, the tire slip angle is constrained in the mostly linear region of the lateral tire force characteristic. By no means does the constraints (16j) enforce the dynamical system to operate in a linear region: system nonlinearities (11) and longitudinal tire nonlinearities are still relevant when constraints (16j) are included in the MPC formulation.

Note that the constraints (16j) are implicit linear constraints on state and input and they can be handled systematically only in an MPC scheme. A soft constraint formulation is preferred to a hard constraint in order to avoid infeasibility. In fact, during experiments the tire slip angle is estimated from IMU and GPS measurements. Acceleration measurements are noisy and the GPS signal can be lost. Moreover, as shown in (3) and (7), the tire slip angle depends on the steering angle. The latter, as explained in Section V-B, in our experimental setup is affected by the driver's imposed steering angle.

An additional tracking error on yaw rate is included in the performance index of the LTV MPC problem (16) and (17) (compare (16d) to (12)). Extensive simulations have shown that this additional term significantly improves the performance of the LTV MPC controller (16) and (17).

V. DOUBLE LANE CHANGE ON SNOW USING ACTIVE STEERING

The MPC steering controllers described in Sections IV-A and IV-B have been implemented to perform a sequence of double lane changes at different entry speeds. This test represents an obstacle avoidance emergency maneuver in which the vehicle is entering a double lane change maneuver on snow or ice with a given initial forward speed. The control input is the front steering angle and the goal is to follow the trajectory as close as possible by minimizing the vehicle deviation from the target path. The experiment is repeated with increasing entry speeds until the vehicle loses control. The same controller can be used to control the vehicle during different maneuvers in different scenarios [21].

The simulation and experimental results will be presented in Section VI. Next, we describe the reference generation and present the experimental setup in Section V-B.

A. Trajectory Generation

The desired path is described in terms of lateral position Y_{ref} and yaw angle ψ_{ref} as function of the longitudinal position X

$$\psi_{\mathrm{ref}}(X) = \frac{d_{y_1}}{2}\left(1 + \tanh(z_1)\right) - \frac{d_{y_2}}{2}\left(1 + \tanh(z_2)\right) \quad (18a)$$

$$\begin{aligned} Y_{\mathrm{ref}}(X) = \arctan\Bigg(& d_{y_1}\left(\frac{1}{\cosh(z_1)}\right)^2\left(\frac{1.2}{d_{x_1}}\right) \\ & - d_{y_2}\left(\frac{1}{\cosh(z_2)}\right)^2\left(\frac{1.2}{d_{x_2}}\right)\Bigg) \end{aligned} \quad (18b)$$

where $z_1 = (2.4/25)(X - 27.19) - 1.2$, $z_2 = (2.4/21.95)(X - 56.46) - 1, 2$, $d_{x_1} = 25$, $d_{x_2} = 21.95$, $d_{y_1} = 4.05$, and $d_{y_2} = 5.7$.

The reference trajectories (18a) and (18b), can be used directly only in the nonlinear MPC formulation, being a nonlinear function of the longitudinal distance X. In the LTV MPC formulation, we generate the reference trajectories from (18a) and (18b) by assuming that the vehicle will travel a portion of the desired path at a constant speed in the next H_p steps.

Because of the assumption on constant travel velocity, the method for generating the previously described trajectory can affect the performance of the closed-loop system. In particular, in extreme handling situations, when the tracking errors are large due to spinning or side skidding, the computed reference could lead to aggressive maneuvers. As explained in Section III, more accurate methods could be used in order to generate a smoother reference for the LTV MPC scheme by taking into account the state of the vehicle.

B. Experimental Setup Description

The MPC controllers presented in Sections IV-A and IV-B have been tested through simulations and experiments on slippery surfaces. The experiments have been performed at a test center equipped with icy and snowy handling tracks. The MPC controllers have been tested on a passenger car, with a mass of 2050 Kg and an inertia of 3344 kg/m^2. The controllers were run

in a dSPACE Autobox system, equipped with a DS1005 processor board and a DS2210 I/O board, with a sample time of 50 ms.

We used an Oxford Technical Solution (OTS) RT3002 sensing system to measure the position and the orientation of the vehicle in the inertial frame and the vehicle velocities in the vehicle body frame. The OTS RT3002, is housed in a small package that contains a differential GPS receiver, inertial measurement unit (IMU), and a DSP. It is equipped with a single antenna to receive GPS information. The IMU includes three accelerometers and three angular rate sensors. The DSP receives both the measurements from the IMU and the GPS, utilizes a Kalman filter for sensor fusion, and calculates the position, the orientation, and other states of the vehicle such as longitudinal and lateral velocities.

The car was equipped with an AFS system which utilizes an electric drive motor to change the relation between the hand steering wheel and road wheel angles. This is done independently from the hand wheel position, thus the front road wheel angle is obtained by summing the driver hand wheel position and the actuator angular movement. Both the hand wheel position and the angular relation between hand and road wheels are measured. The sensor, the dSPACE Autobox, and the actuators communicate through a CAN bus.

The autonomous steering test is initiated by the driver with a button. When the button is pushed, the inertial frame in Fig. 1 is initialized as follows: the origin is the current vehicle position, the axes X and Y are directed as the current longitudinal and lateral vehicle axes, respectively. Such inertial frame becomes also the desired path coordinate system. Once the initialization procedure is concluded, the vehicle executes the double lane change maneuver.

During the experiment, the hand wheel may deviate from its center position. This is caused by the difficulty the driver can have in holding the steering still, which was needed to facilitate autonomous behavior with that particular test vehicle. In our setup, this is treated as a small bounded input disturbance. Furthermore, noise may affect the yaw angle measurement due to the single antenna sensor setup. Compared to a dual antenna setup, a single antenna system has to learn the vehicle orientation and/or coordinate during vehicle motion. When the vehicle stands still the yaw angle is computed by integrating the yaw rate measurement from the IMU. This might cause the presence of a small offset in the orientation measurement, while traveling at low speed or being still. The effects of both input disturbance and measurement noise will be clear later in the presented experimental results.

VI. PRESENTATION AND DISCUSSION OF RESULTS

In Section VI-A, three types of MPC controllers will be presented. These controllers have been derived by the MPC problem formulations presented in Sections IV-A and IV-B and will be referred to as Controller A, B, and C.

- Controller A: Nonlinear MPC (14) and (15) with the following parameters:
  - $T = 0.05$ s, $H_p = 7$; $H_c = 3$; $\delta_{f,\min} = -10°$, $\delta_{f,\max} = 10°$, $\Delta\delta_{f,\min} = -1.5°$, $\Delta\delta_{f,\max} = 1.5°$, $\mu = 0.3$;
  - $Q = \begin{pmatrix} 500 & 0 \\ 0 & 75 \end{pmatrix}$, $R = 150$.

TABLE I
MAXIMUM COMPUTATION TIME OF CONTROLLERS A AND B PERFORMING
A DOUBLE LANE CHANGE MANEUVER AT DIFFERENT VEHICLE SPEEDS

$\dot{x}$ [m/s]	Controller A Comp. time [s]	Controller B Comp. time [s]
10	0.15 ($H_p = 7, H_c = 2$)	0.03 ($H_p = 7, H_c = 3$)
15	0.35 ($H_p = 10, H_c = 4$)	0.03 ($H_p = 10, H_c = 4$)
17	1.3 ($H_p = 10, H_c = 7$)	0.03 ($H_p = 15, H_c = 10$)

- Controller B: LTV MPC (16) and (17) with the following parameters:
  - $T = 0.05$ s, $H_p = 25$; $H_c = 10$, $\delta_{f,\min} = -10°$, $\delta_{f,\max} = 10°$, $\Delta\delta_{f,\min} = -0.85°$, $\Delta\delta_{f,\max} = 0.85°$, $\mu = 0.3$, $\alpha_{\min} = -2.2°$, $\alpha_{\max} = 2.2°$;
  - weighting matrices $Q = \begin{pmatrix} 200 & 0 & 0 \\ 0 & 10 & 0 \\ 0 & 0 & 10 \end{pmatrix}$, $R = 5 \cdot 10^4$, $\rho = 10^3$.
- Controller C: Same as Controller B with $H_c = 1$.

Next, the results obtained with the three controllers will be described and a comparison between the simulation and the experimental results will be given for each of them. The actual road friction coefficient μ was set manually and constant for each experiment depending on the road conditions. This choice was driven by the study of the controller closed-loop performance independently from the μ estimation and its associated error and dynamics. *For each controller more simulation, experiments, and comments can be found in* [12].

A. Controller A

The controller (14) and (15) with the parameters defined in Section VI has been implemented as a C-coded S-function in which the commercial NPSOL software package [15] is used for solving the nonlinear programming problem (14). The choice of NPSOL has been motivated by its performance and the availability of the source C code.

Limited by the computational complexity of the nonlinear programming solver and the hardware used, we could perform experiments at low vehicle speeds only. In fact, as the entry speed increases, larger prediction and control horizons are required in order to stabilize the vehicle along the path. Larger prediction horizons involve more evaluations of the objective function, while larger control horizons imply a larger optimization problem (14). In Table I, we report the maximum computation time required by the Controllers A and B to compute a solution to the problems (14) and (16), respectively, when the maneuver described in Section V is performed at different vehicle speeds. The selected control and prediction horizons in Table I are the shortest allowing the stabilization of the vehicle at each speed. The results have been obtained in simulation with a 2.0-GHz Centrino-based laptop running Matlab 6.5.

During experiments, the maximum iterations number in NPSOL bas been limited in order to guarantee real-time computation. The bound was selected after preliminary tests on the real-time hardware.

In Fig. 4, the simulation results for a maneuver at 7 m/s are presented. In Fig. 5, the corresponding experimental results are presented. In the upper plot of Fig. 5(b), the dashed line represents the steering action from the driver (i.e., the input disturbance) that, in this test, is negligible. The actual road wheel
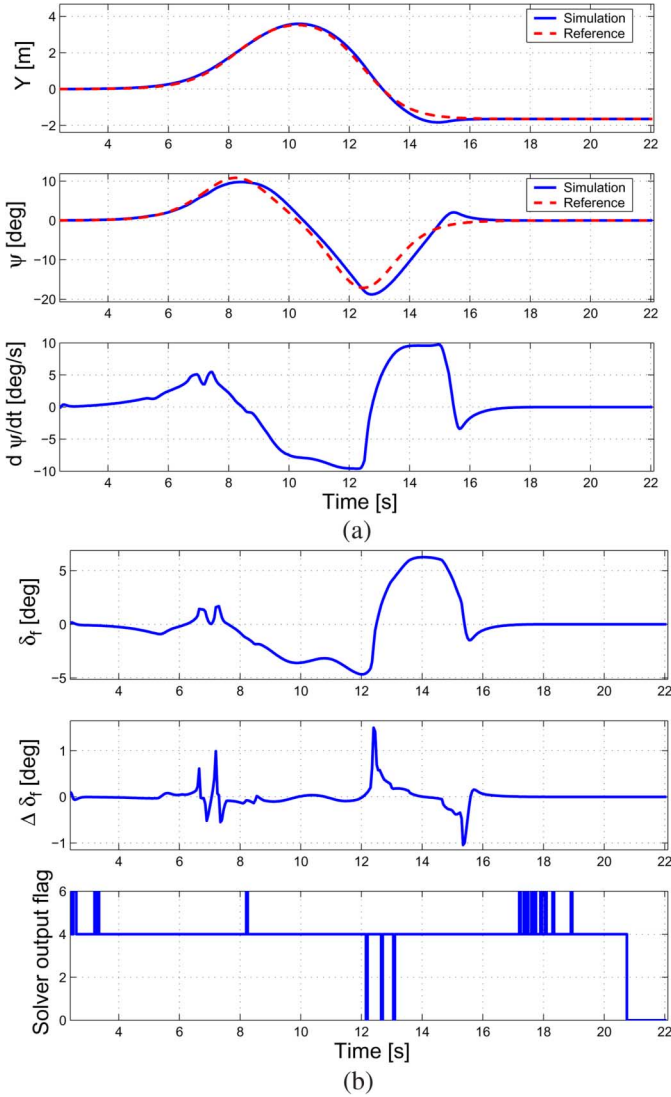
Fig. 4. Simulation results at 7-m/s entry speed. Controller A described in Section IV-A. (a) Lateral position (Y), yaw angle (ψ), and yaw rate $\dot{\psi}$. (b) Front steering angle (δ_f), change in front steering angle $(\Delta\delta_f)$, and NPSOL output flag.

Fig. 5. Experimental results at 7-m/s entry speed. Controller A described in Section VI-A. (a) Lateral position (Y), yaw angle (ψ), and yaw rate $\dot{\psi}$. (b) Front steering angle (δ_f), change in front steering angle $(\Delta\delta_f)$, and NPSOL output flag.

angle (RWA) is the summation of the RWA from the MPC controller and the steering action from the driver. In lower plots of Figs. 4(b) and 5(b), the NPSOL output flag is reported. In our tests, the flag assumed the values 0, 1, 4, and 6. The value 0 is returned when an optimal feasible solution is found. The value 1 is returned when the solver does not converge to a feasible solution. The value 4 indicates that the limit on the iteration number has been reached and a feasible but nonoptimal solution has been found. The value 6 indicates that the solution does not satisfy the optimality conditions [15]. In simulation and experimental tests, the solver often reaches the selected iteration limit and returns a suboptimal solution. Yet, because of the low vehicle speed, the performance associated to the suboptimal solution is excellent.

By comparing the lateral position and yaw angle in the simulation and the experiment, we can conclude that the matching between simulation and experimental results is very good. The tracking errors are very small and reported in Table II, where
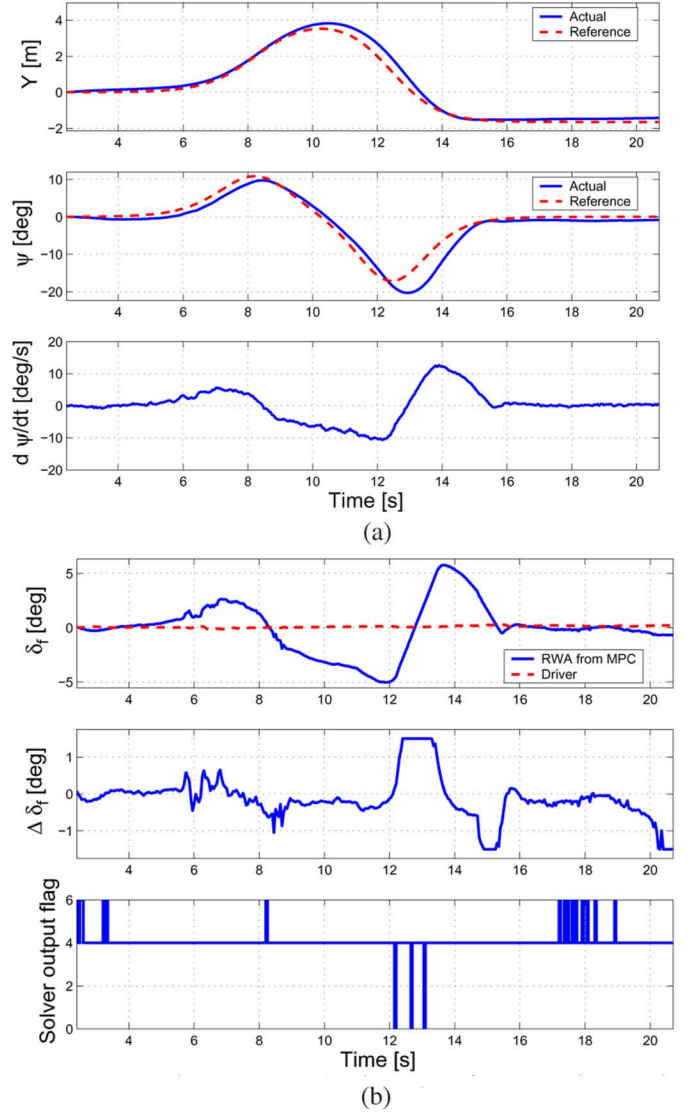
ψ_{rms} and Y_{rms} are the root mean squared (rms) yaw angle and lateral position tracking errors, respectively. The values of $\psi_{\max}$ and $Y_{\max}$ are the maximum tracking errors on the same variables.

By comparing the simulated and the experimental steering command, we notice the presence of an unmodeled rate saturation in the steering response. In fact, the actual road steering angle variation is smaller than the selected $\Delta\delta_{f,\max}$ in (14g). This can be observed in Fig. 5(b), between 12 and 14 s, where the desired change in the steering angle was limited to $\Delta\delta_{f,\max} = 1.5°$, while the actual road wheel steering angle increased at a slower rate. This led to a larger tracking error in the experiment during the second lane change compared to the simulations.

The experimental results 10 m/s in [12] show that the controller is not able to stabilize the vehicle and, around 13 s, the vehicle starts to skid. The controller fails because the nonlinear solver does not converge to a feasible solution.

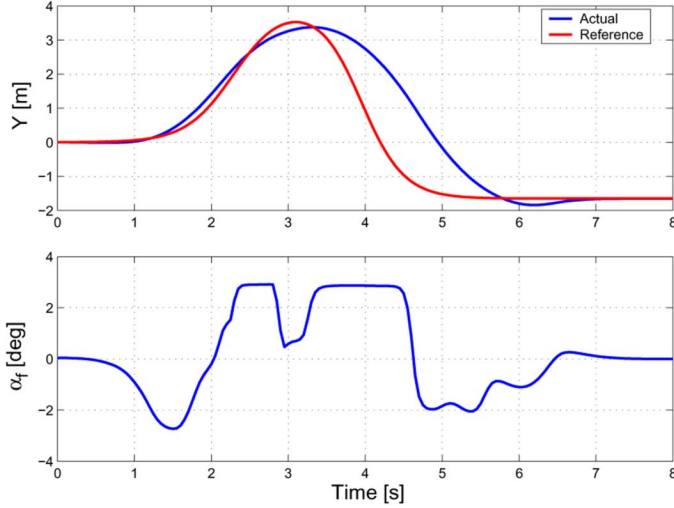|	ψ_{rms} [deg]	Y_{rms} [m]	ψ_{max} [deg]	Y_{max} [m]
Simulation	$1.05 \cdot 10^{-1}$	$6.36 \cdot 10^{-4}$	4.20	$3.82 \cdot 10^{-1}$
Experiment	$2.26 \cdot 10^{-1}$	$3.50 \cdot 10^{-3}$	6.99	$7.43 \cdot 10^{-1}$

Fig. 6.   Simulation results of Controller A at 17 m/s.

Fig. 7.   Simulation results at 10-m/s entry speed. Controller B described in Section IV-B. (a) Lateral position (Y), yaw angle (ψ), and yaw rate $\dot{\psi}$. (b) Front steering angle (δ_f), change in front steering angle $(\Delta \delta_f)$, and front tire slip angle α_f.

An analysis of simulation results shows that the solver does not converge because of the limit on the number of iterations. The work presented in [7] has shown that, the NL-MPC controller is able to perform the maneuver at 10-m/s or higher speed if the solver maximum iteration number is not limited.

Finally, in order to better motivate the introduction of the constraints (16j) in the MPC formulation presented in Section IV-B, in Fig. 6, we report the simulation results of a nonlinear MPC at 17 m/s on snow. We observe that, due to the knowledge of the tire characteristics, the controller implicitly limits the front tire slip angle (α_f) in the interval $[-3, +3]^\circ$. As shown in Fig. 2, this is within the linear region of the tire characteristic for a snow covered road $(\mu = 0.3)$. The results in Fig. 6 have been obtained by Controller A using the same tuning parameters of Controller B presented in Section VI. In particular, a prediction horizon of 25 steps and a control horizon of ten steps have been selected. The steering angle has been constrained within the interval $[-10, 10]^\circ$, while the steering rate in $[-0.85, 0.85]^\circ$. We also point out that no constraint on the front tire slip angle has been used.

Extensive simulations have shown that this phenomenon can always be observed in extreme conditions under operations and led us to the use of the constraint (16j) in the LTV MPC formulation (16).

B. Controller B

The controller (16) and (17) with the parameters defined in Section VI has been implemented as a C-coded S-Function, using the QP solver routine available in [32]. Such routine implements the Dantzig–Wolfe's algorithm, has a good performance and its source C code is publicly available. We do not report the solver output flag since the solve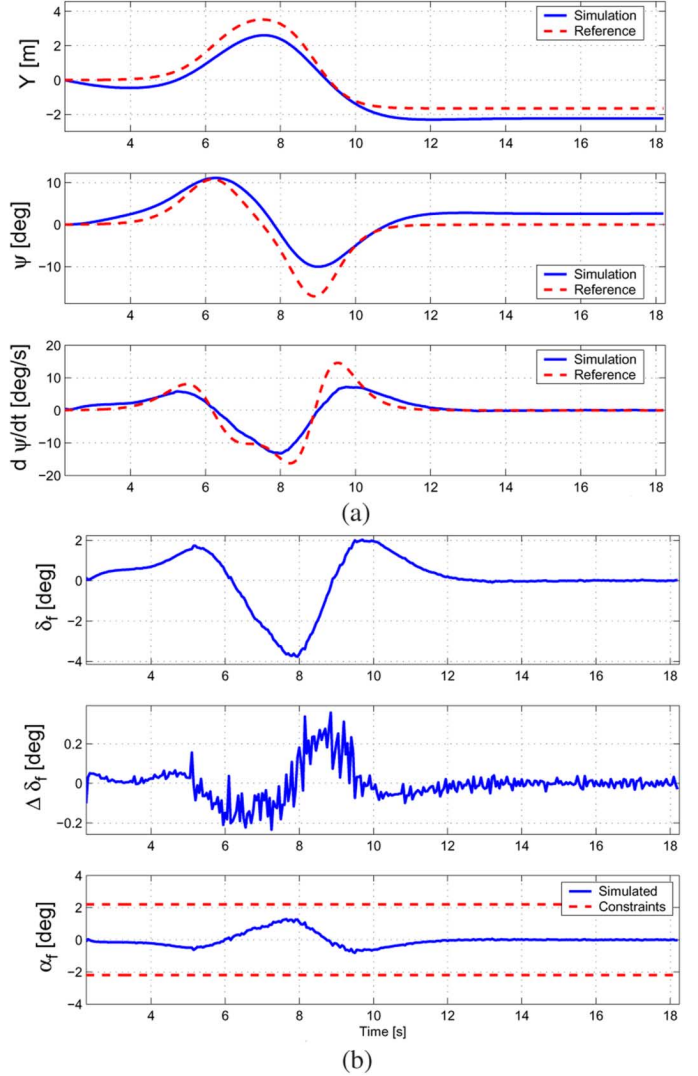r always converged to an optimal solution. At each time step, the linear model (16b) and (16c) is obtained by analytic differentiation of the nonlinear vehicle model (11) and a numeric linearization of the Pacejka tire model.

We remark that the computation burden of this LTV MPC controller is reduced significantly compared to the controller presented in Section VI-A, as demonstrated by the computation times reported in Table I.

Fig. 7 depicts simulation results at the entry speed of 10 m/s. Table III summarizes the tracking errors obtained in simulation for entry speeds of 10 to 21.5 m/s. In Fig. 7(a), one can observe: 1) an undershoot in the lateral position and 2) steady-state errors in both lateral position and yaw angle. Moreover, the steady-state values of the position and the yaw angle are not coherent, being the lateral position is constant and the yaw angle is nonzero. These phenomena are generated by an orientation error, detected in the experimental data and introduced in the presented simulations in order to fairly compare the simulation and the experimental results. For each simulation, the introduced orientation error is reported in the last column of Table III.

TABLE III
SIMULATION RESULTS. CONTROLLER B PRESENTED IN
SECTION VI-B. rms AND MAXIMUM TRACKING ERRORS AS
FUNCTION OF VEHICLE LONGITUDINAL SPEED

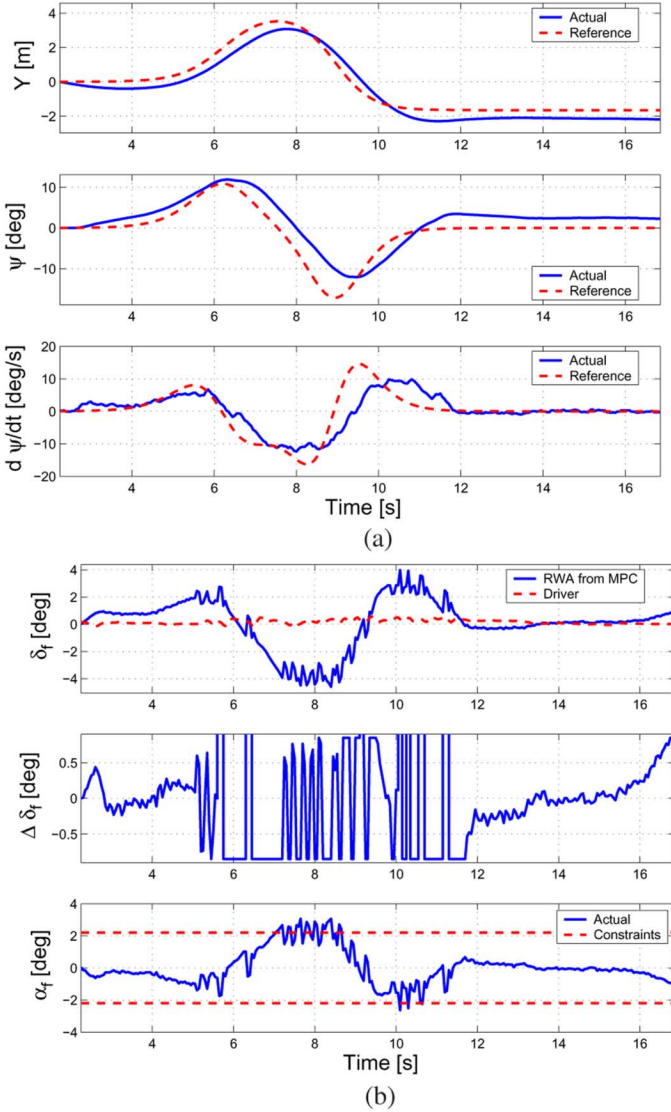| $\dot{x}$ [m/s]	μ	ψ_{rms} [deg]	Y_{rms} [m]	ψ_{max} [deg]	Y_{max} [m]	Δ [deg]
10	0.3	0.39	$1.77 \cdot 10^{-2}$	7.20	0.96	2.6
15	0.3	0.41	$2.56 \cdot 10^{-2}$	8.17	1.25	2.67
19	0.3	0.42	$3.03 \cdot 10^{-2}$	10.15	1.58	2.33
21.5	0.25	0.68	$5.41 \cdot 10^{-2}$	11.61	2.11	2.85

Fig. 8. Experimental results at 10-m/s entry speed. Controller B described in Section VI-B. (a) Lateral position (Y), yaw angle (ψ), and yaw rate $\dot{\psi}$. (b) Front steering angle (δ_f), change in front steering angle $(\Delta\delta_f)$, and front tire slip angle α_f.

The orientation error is due to a measurement offset in the yaw signal coming from the OTS sensor. The effects of this error will be clarified and described in detail in Section VI-C. In the lower plot of Fig. 7(b) the front tire slip angle is reported.

In Fig. 8, the experimental results at 10 m/s are presented. By comparing these results with the simulations at the same speed shown in Fig. 7(a) and (b), we observe a good matching between
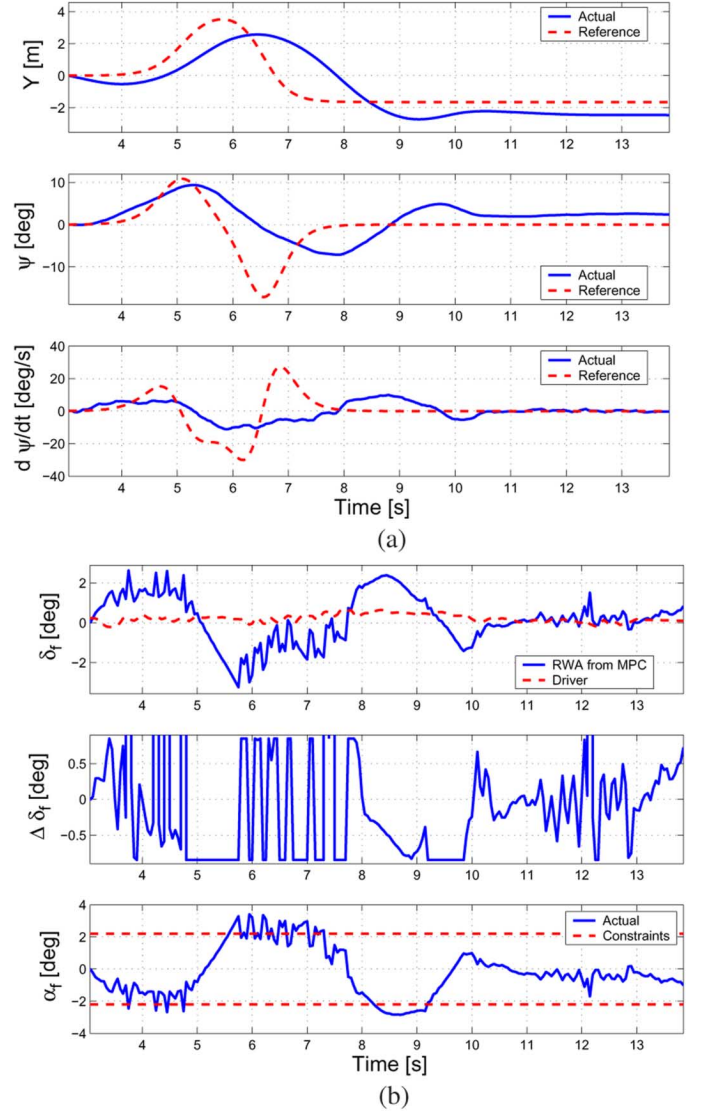

Fig. 9. Experimental results at 19-m/s entry speed. Controller B described in Section VI-B. (a) Lateral position (Y), yaw angle (ψ), and yaw rate $\dot{\psi}$. (b) Front steering angle (δ_f), change in front steering angle $(\Delta\delta_f)$, and front tire slip angle α_f.

experiments and simulations. We also observe a chattering phenomenon in the signals $\Delta\delta_f$ and δ_f. This is a function of the MPC tuning and of the constraints $\Delta\delta_{f,\max}$ and $\Delta\delta_{f,\min}$. No additional effort has been spent in reducing such phenomenon since it is mostly filtered by the vehicle response and not felt by the driver.

For all experimental results presented in the following, the slip angle has been computed using the experimental data and (3), (4), and (7).

In Fig. 9, the experimental results at 19 m/s are presented. By comparing the lateral positions in Figs. 8(a) and 9(a) at 10 and 19 m/s, respectively, we observe a larger error in the lateral position at 19 m/s, between 6 and 8 s at the beginning of the second lane change. A postprocessing of experimental data and the analysis of simulation data have shown that the constraint (16j) on the tire slip angle corresponds to an implicit constraint on the maximum steering action which decreases with the higher longitudinal vehicle speeds. The commanded wheel steering angle when the

TABLE IV
CONTROLLER B PRESENTED IN SECTION VI-B. EXPERIMENTAL
RMS AND MAXIMUM TRACKING ERRORS AS FUNCTION
OF VEHICLE LONGITUDINAL SPEED

$\dot{x}$ [m/s]	μ	ψ_{rms} [deg]	Y_{rms} [m]	ψ_{max} [deg]	Y_{max} [m]
10	0.3	0.53	$1.28 \cdot 10^{-2}$	8.21	0.8
15	0.3	1.172	$4.64 \cdot 10^{-2}$	14.71	2.51
19	0.3	1.23	$7.51 \cdot 10^{-2}$	16.38	3.10
21.5	0.25	1.81	$1.11 \cdot 10^{-1}$	19.02	2.97

slip angle is at its lower bound $(-2.2°)$ decreases with the vehicle longitudinal speed.

We remark that in almost all experimental tests the tire slip angle violates its constraint in a small amount. This is in agreement with the use of soft constraint and makes the system robust to driver steering action, as it can be seen in Fig. 9 between 8 and 9 s.

The presented experimental results are summarized in Table IV. The comparison between simulation and experimental results, in Tables III and IV, respectively, demonstrates that, in spite of a significant model mismatch at high speeds, vehicle stability is achieved in all experimental tests. This is enforced by the constraints (16j) which mitigates the effect of model uncertainties. The mismatch between the closed- and the open-loop behavior resides in the uncertainty in the tire characteristics. Such mismatch led to a conservative choice for the slip angle constraints in the experimental tests. As a direct consequence, the steering angle has been implicitly overconstrained in experiments at high vehicle speed with a consequent performance degradation. This can be observed in the experimental tests at the second lane change, where the error in the lateral position becomes large compared to the simulation results.

By comparing the simulation and experimental results at 10 m/s in Tables III and IV, respectively, it can be observed that the experimental rms lateral error is lower than the corresponding simulative result. In fact, a different equilibrium point is reached in the two cases. Section VI-C clarifies the cause of mismatch between simulative and experimental equilibrium point.

As remarked in previous sections, Controller B performance degrades when the constraint (16j) on the tire slip angle is removed. In this case, extensive simulations have shown that the LTV MPC controller is able to stabilize the vehicle only up to 10 m/s.

C. Steady-State Errors

In this section, we will explain the initial undershoot in the lateral position and the steady-state errors in both lateral position and yaw angle observed in the presented experimental results of Controller B. As previously mentioned, both phenomena are caused by an offset on the orientation measurement. Fig. 10 reproduces the scenario: the axes x_{act} and y_{act} are the actual longitudinal and lateral vehicle axes, respectively, while x_{lea} and y_{lea} are the vehicle axes as learned by the OTS sensor.

Because of a positive orientation error, at the beginning of the test the sensor measures a zero yaw angle while the actual vehicle longitudinal axis points rightwards, as shown in Fig. 10(a).
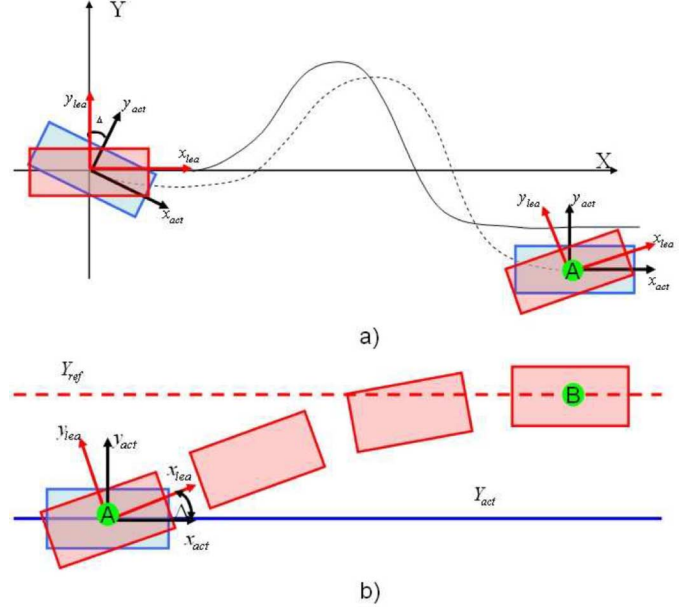

Fig. 10. Effects of the orientation error on lateral position and yaw angle. (a) Undershoot in the lateral position. (b) Steady-state error on lateral position and yaw angle.

This explains the initial undershoot in the lateral position. At the end of the maneuver (position A in Fig. 10(a)), the vehicle is actually going straight, as confirmed by the constant lateral position and zero steering angle, while the measured nonzero yaw angle is exactly the orientation error, as illustrated in Fig. 10(a).

Consider Figs. 8, 9, and 11, in spite of the steady-state errors on both lateral position and yaw angle, the MPC controller does not attempt to reduce the errors on tracking variables. The explanation is simple: because of the offset on the yaw measurement, any attempt to reduce the yaw angle (lateral position) tracking error would imply an increase of the lateral position (yaw angle) tracking error according to model (2). Since the proposed MPC does not contain any integral action, the steady-state equilibria which can be observed in Figs. 8, 9, and 11 are the closed-loop optimal equilibria for the designed MPC. The simulation results in Fig. 7 reproduces exactly the steady-state offset observed in experiments and confirm our explanation. We remark that an MPC controller with integral action on the tracking errors would have led to an unstable vehicle behavior. In fact, due to the inconsistency between the orientation and position measurements, a zero steady-state orientation error would have implied a diverging lateral position.

D. Controller C

The controller (16) and (17) with the parameters defined in Section VI has been implemented as a C-coded S-function, by using a very simple QP solver for a 2-D problem. Since $H_c = 1$, the two optimization variables are the commanded steering variation and the slack variable. We implemented a tailored QP solver.

The plot of the simulation results are not included in this manuscript because of lack of space. We only report, in Table V, the tracking errors at 10-, 15-, 19-, and 21-m/s entry speeds. The experimental results of controller C at 10, 17, and 21 m/s are
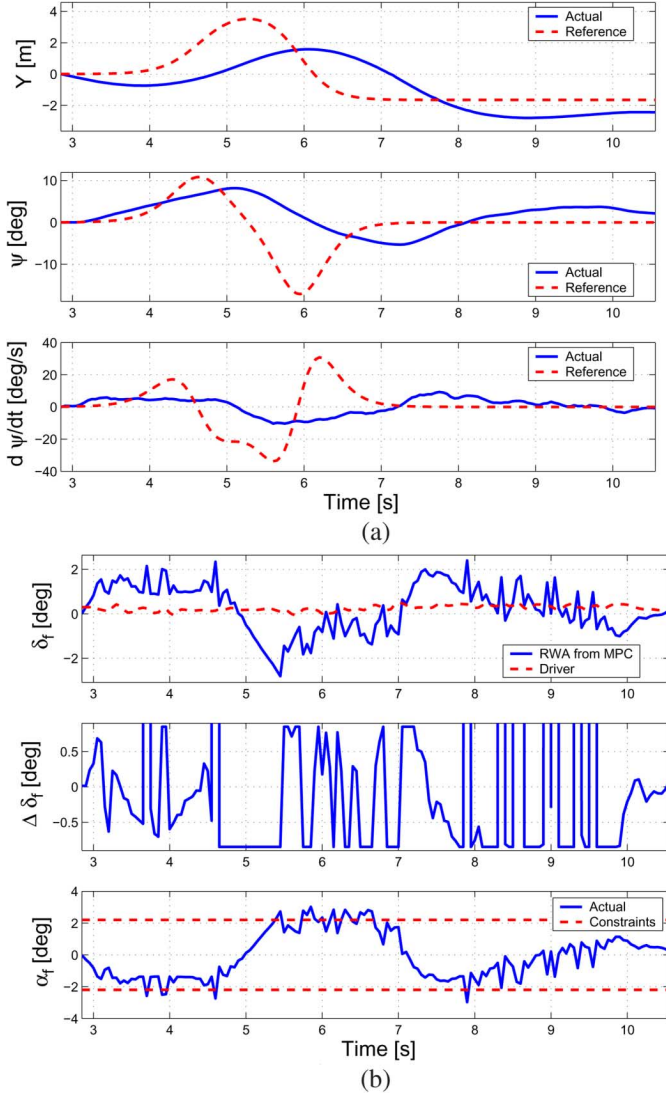
Fig. 11. Experimental results at 21.5-m/s entry speed. Controller B described in Section VI-B. (a) Lateral position (Y), yaw angle (ψ), and yaw rate $\dot{\psi}$. (b) Front steering angle (δ_f), change in front steering angle ($\Delta\delta_f$), and front tire slip angle α_f.

TABLE V
SUMMARY OF SIMULATION RESULTS, CONTROLLER C PRESENTED IN
SECTION VI-D. SIMULATIVE RMS AND MAXIMUM TRACKING
ERRORS AS FUNCTION OF VEHICLE LONGITUDINAL SPEED.
THE ORIENTATION ERRORS HAVE BEEN REPRODUCED

$\dot{x}$ [m/s]	μ	ψ_{rms} [deg]	Y_{rms} [m]	ψ_{max} [deg]	Y_{max} [m]
10	0.3	$4.40 \cdot 10^{-1}$	$2.30 \cdot 10^{-2}$	7.98	1.07
15	0.3	$4.76 \cdot 10^{-2}$	$3.56 \cdot 10^{-2}$	9.56	1.50
19	0.3	$5.09 \cdot 10^{-1}$	$4.68 \cdot 10^{-2}$	11.61	1.89
21	0.25	$7.20 \cdot 10^{-1}$	$7.70 \cdot 10^{-2}$	12.26	2.34

TABLE VI
SUMMARY OF EXPERIMENTAL RESULTS, CONTROLLER C PRESENTED
IN SECTION VI-D. RMS AND MAXIMUM TRACKING ERRORS
AS FUNCTION OF VEHICLE LONGITUDINAL SPEED

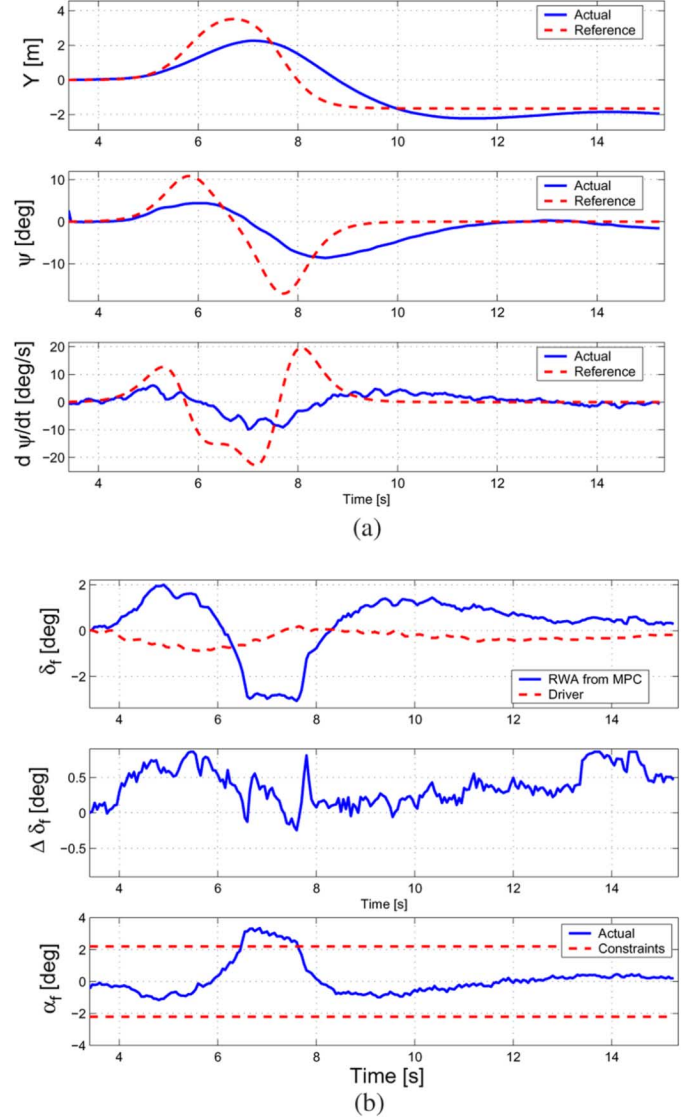| $\dot{x}$ [m/s]	μ	ψ_{rms} [deg]	Y_{rms} [m]	ψ_{max} [deg]	Y_{max} [m]
10	0.2	$9.52 \cdot 10^{-1}$	$5.77 \cdot 10^{-2}$	13.12	3.28
17	0.25	$8.28 \cdot 10^{-1}$	$2.90 \cdot 10^{-2}$	12.26	1.81
21	0.2	1.037	$7.66 \cdot 10^{-2}$	12.49	3.20

Fig. 12. Experimental results at 17 m/s entry speed. Controller C described in Section VI-D. (a) Lateral position (Y), yaw angle (ψ), and yaw rate $\dot{\psi}$. (b) Front steering angle (δ_f), change in front steering angle ($\Delta\delta_f$), and front tire slip angle α_f.

summarized in Table VI, the results at 17 m/s are presented in Fig. 12.

The plots results do not show any orientation error, being the experiments performed in a day different from experiments of controller B. It is interesting to observe that, even if the control horizon has been tightened significantly, the controller is still able to stabilize the vehicle, even at high speed, and the tracking errors do not increase significantly compared to Controller B.

In order to fairly compare Controllers B and C, the orientation offset observed during experimental tests of Controller B have been reproduced in simulations of Controller C. The tracking errors for such simulation are reported in Table V. Compare the tracking errors of Controllers B and C in Tables III and V, respectively. It can be noticed that Controller C performs slightly worse than Controller B. However, as confirmed by the experimental tests, it is able to stabilize the vehicle at high speed.

We emphasize that such an MPC controller can be implemented on a low-cost hardware and its code can be easily verified. The maximum number of operation at each time step is also easily computed whereas this can be very difficult for Controllers B and C.

VII. CONCLUSION

We have presented a novel MPC-based approach for active steering control design. Experimental results showed that double lane change maneuvers are relatively easily obtained as a result of the MPC feedback policy, leading to the capability of stabilizing a vehicle with a speed up to 21 m/s on slippery surfaces such as snow covered roads.

There are three main contributions of this manuscript. These are associated with the three types of MPC controllers which have been designed and experimentally tested. First, a nonlinear MPC has been designed and implemented on a rapid prototyping system. Because of computational burden, experimental tests could be performed only at low vehicle speed on the available hardware. Yet, to the best of our knowledge, for the first time a nonlinear MPC scheme has been implemented on a dSPACE rapid prototyping system to control the vehicle dynamics of an autonomous passenger car with a frequency of 20 Hz. Second, an LTV MPC has been designed and implemented. The use of a state and input constraint on the tire slip angle has been proposed in order to stabilize the vehicle at high speeds. Its effectiveness has been shown through simulations and experiments. Both approaches suffer from the difficulty in verifying the optimization code and computing the worst case computational time. The third and last contribution overcomes these issues and it is represented by an LTV MPC controller of low order which shows acceptable performance and can be easily implemented in a low cost hardware.

The results presented here open the route to interesting and challenging research activities, which are the current topic of ongoing work. From a computational point of view, we are improving and testing several nonlinear optimization algorithms which can enlarge the range of conditions for which a nonlinear MPC becomes real-time implementable. From a control design point of view, we are studying new control paradigms in order to achieve similar performance to the nonlinear MPC with a significant reduction of the computational burden. We are also studying the stability and the robustness of the proposed LTV MPC scheme. From an application point of view, we are increasing the number of control inputs and working on multi-variable vehicles dynamic control schemes controlling steering, brakes, and throttle.

REFERENCES

[1] J. Ackermann, D. Odenthal, and T. Bünte, "Advantages of active steering for vehicle dynamics control," in *Proc. 32nd Int. Symp. Autom. Technol. Autom.*, 1999, pp. 263–270.

[2] J. Ackermann and W. Sienel, "Robust yaw damping of cars with front and rear wheel steering," *IEEE Trans. Control Syst. Technol.*, vol. 1, no. 1, pp. 15–20, Mar. 1993.

[3] J. Ackermann, W. Walter, and T. Bünte, "Automatic car steering using robust unilateral decoupling," presented at the Int. Conf. Adv. Veh. Control Safety, Genoa, Italy, 2004.

[4] E. Bakker, L. Nyborg, and H. B. Pacejka, "Tyre modeling for use in vehicle dynamics studies," SAE Int., Warrendale, PA, 870421, 1987.

[5] R. Behringer, B. Gregory, V. Sundareswaran, R. Addison, R. Elsley, W. Guthmiller, and J. Demarche, "Development of an autonomous vehicle for the DARPA grand challenge," presented at the IFAC Symp. Intell. Autonomous Veh., Lisbon, Portugal, 2004.

[6] F. Borrelli, A. Bemporad, M. Fodor, and D. Hrovat, "An MPC/hybrid system approach to traction control," *IEEE Trans. Control Syst. Technol.*, vol. 14, no. 3, pp. 541–552, May 2006.

[7] F. Borrelli, P. Falcone, T. Keviczky, J. Asgari, and D. Hrovat, "MPC-based approach to active steering for autonomous vehicle systems," *Int. J. Veh. Autonomous Syst.*, vol. 3, no. 2/3/4, pp. 265–291, 2005.

[8] PC. Calhoun and EM. Queen, "Entry vehicle control system design for the mars smart lander," presented at the AIAA Atmospheric Flight Mech. Conf., Monterey, CA, 2002.

[9] L. Chisci, P. Falugi, and G. Zappa, "Gain-scheduling MPC of nonlinear systems," *Int. J. Robust Nonlinear Control*, vol. 13, pp. 295–308, 2003.

[10] T. Costlow, "Active safety," SAE Int., Warrendale, PA, 2005.

[11] dSPACE GmbH, "dSPACE autobox," Paderborn, Germany, 2006.

[12] P. Falcone, F. Borrelli, J. Asgari, H. E. Tseng, and D. Hrovat, "Predictive active steering control for autonomous vehicle systems," Dipartimento di Ingegneria, Universitá del Sannio, Benevento, Italy, (2007). [Online]. Available: http://www.grace.ing.unisannio.it/publication/416

[13] R. E. Fenton, G. C. Melocik, and K. W. Olson, "On the steering of automated vehicles: Theory and experiments," *IEEE Trans. Autom. Control*, vol. AC-21, no. 3, pp. 306–315, Jun. 1976.

[14] C. E. Garcia, D. M. Prett, and M. Morari, "Model predictive control: Theory and practice-A survey," *Automatica*, vol. 25, pp. 335–348, 1989.

[15] P. Gill, W. Murray, M. Saunders, and M. Wright, *NPSOL—Nonlinear Programming Software*. Mountain View, CA: Stanford Business Software, Inc., 1998.

[16] J. Guldner, W. Sienel, H. S. Tan, J. Ackermann, S. Patwardhan, and T. Bünte, "Robust automatic steering control for look-down reference systems with front and rear sensors," *IEEE Trans. Control Syst. Technol.*, vol. 7, no. 1, pp. 2–11, Jan. 1999.

[17] D. Hrovat, "MPC-based idle speed control for IC engine," presented at the FISITA, Prague, Czech Republic, 1996.

[18] T. Keviczky and G. J. Balas, "Flight test of a receding horizon controller for autonomous uav guidance," in *Proc. Amer. Contr. Conf.*, 2005, pp. 3518–3523.

[19] ——, "Receding horizon control of an f-16 aircraft: A comparative study," *Control Eng. Practice*, vol. 14, no. 9, pp. 1023–1033, Sep. 2006.

[20] ——, "Software-enabled receding horizon control for autonomous UAV guidance," *AIAA J. Guid., Control, Dyn.*, vol. 29, no. 3, pp. 680–694, May/Jun. 2006.

[21] T. Keviczky, P. Falcone, F. Borrelli, J. Asgari, and D. Hrovat, "Predictive control approach to autonomous vehicle steering," in *Proc. Amer. Contr. Conf.*, 2006, pp. 4670–4675.

[22] M. V. Kothare, B. Mettler, M. Morari, P. Bendotti, and C. M. Falinower, "Level control in the steam generator of a nuclear power plant," *IEEE Trans. Control Syst. Technol.*, vol. 8, no. 1, pp. 55–69, Jan. 2000.

[23] T. B. Foote, L. B. Cremean, J. H. Gillula, G. H. Hines, D. Kogan, K. L. Kriechbaum, J. C. Lamb, J. Leibs, L. Lindzey, C. E. Rasmussen, A. D. Stewart, J. W. Burdick, and R. M. Murray, "Alice: An information-rich autonomous vehicle for high-speed desert navigation," *J. Field Robot.*, 2006, submitted for publication.

[24] W. M. Lu and D. S. Bayard, "Guidance and control for mars atmospheric entry: Adaptivity and robustness," Jet Propulsion Lab., Pasadena, CA, 1997.

[25] D. L. Margolis and J. Asgari, "Multipurpose models of vehicle dynamics for controller design," SAE Int., Warrendale, PA, 1991.

[26] D. Q. Mayne, J. B. Rawlings, C. V. Rao, and P. O. M. Scokaert, "Constrained model predictive control: Stability and optimality," *Automatica*, vol. 36, no. 6, pp. 789–814, Jun. 2000.

[27] M. Morari and J. H. Lee, "Model predictive control: Past, present and future," *Comput. Chem. Eng.*, vol. 23, no. 4–5, pp. 667–682, 1999.

[28] E. Ono, S. Hosoe, H. D. Tuan, and S. Doi, "Bifurcation in vehicle dynamics and robust front wheel steering control," *IEEE Trans. Control Syst. Technol.*, vol. 6, no. 3, pp. 412–420, May 1998.

[29] J. Hauser, R. M. Murray, A. Jadbabaie, M. B. Miliam, N. Petit, W. B. Dunbar, and R. Franz, "Online control customization via optimization-based control," in *Software-Enabled Control: Information Technology for Dynamical Systems*. Piscataway, NJ: IEEE Press, 2003.

[30] M. Montemerlo, S. Thrun, H. Dahlkamp, D. Stavens, A. Aron, J. Diebel, P. Fong, J. Gale, M. Halpenny, G. Hoffmann, K. Lau, C. Oakley, M. Palatucci, V. Pratt, P. Stang, S. Strohband, C. Dupont, L.-E. Jendrossek, C. Koelen, C. Markey, C. Rummel, J. van Niekerk, E. Jensen, P. Alessandrini, G. Bradski, B. Davies, S. Ettinger, A. Kaehler, A. Nefian, and P. Mahoney, "Stanley the robot that won the DARPA grand challenge," *J. Field Robot.*, accepted for publication.

[31] R. R. S. Smith, K. Mease, D. S. Bayard, and D. L. Farless, "Aeromaneu-vering in the martian atmosphere: Simulation-based analyses," *AIAA J. Spacecraft Rockets*, vol. 37, no. 1, pp. 139–142, 2000.

[32] "Model predictive control toolbox" Inc. The MathWorks, Natick, MA, 2005.

[33] P. Tøndel and T. A. Johansen, "Control allocation for yaw stabilization in automotive vehicles using multiparametric nonlinear programming," in *Proc. Amer. Contr. Conf.*, 2005, pp. 453–458.

[34] H. E. Tseng, J. Asgari, D. Hrovat, P. Van Der Jagt, A. Cherry, and S. Neads, "Evasive maneuvers with a steering robot," *Veh. Syst. Dyn.*, vol. 43, no. 3, pp. 197–214, Mar. 2005.

[35] Z. Wan and M. V. Kothare, "Efficient scheduled stabilizing model pre-dictive control for constrained nonlinear systems," *Int. J. Robust Non-linear Control*, vol. 13, pp. 331–346, Mar./Apr. 2003.

[36] W. Zhang and R. E. Parsons, "An intelligent roadway reference system for vehicle lateral guidance/control," in *Proc. Amer. Contr. Conf.*, 1990, pp. 281–286.

Paolo Falcone received the Laurea degree in com-puter science engineering from the University of Naples "Federico II," Naples, Italy, in 2003. He is currently pursuing the Ph.D. degree in automatic control engineering at the "Universita del Sannio," Benevento, Italy.

His research interests include model predictive control and vehicle dynamics control.

Francesco Borrelli received the Laurea degree in computer science engineering from the University of Naples "Federico II," Naples, Italy, in 1998, and the Ph.D. degree in automatic control from ETH Zurich, Zurich, Switzerland, in 2002.

He is currently an Assistant Professor at the "Universiť del Sannio," Benevento, Italy. He was a Re-search Assistant at the Automatic Control Labora-tory, ETH Zurich, and a Contract Assistant Professor at the Aerospace and Mechanics Department, Univer-sity of Minnesota, MN. He is the author of the book *Constrained Optimal Control of Linear and Hybrid Systems* (Springer–Verlag, 2003). His research interests include constrained optimal control, model pre-dictive control, robust control, parametric programming, singularly perturbed systems, and automotive applications of automatic control.

Mr. Borrelli was a recipient of the "Innovation Prize 2004" from the Elec-troSwiss Foundation.

Jahan Asgari has received the B.S.M.E. degree from California State University, Sacramento, in 1983, and the M.S. and Ph.D. degrees from University of Cali-fornia, Davis, in 1985 and 1989, respectively.

Since then, he has been working at Research and Advance Engineering Department, Ford Motor Com-pany, Dearborn, MI, where his activities include sev-eral projects in the area of driveline and chassis mod-eling, control, and optimization.

Hongtei Eric Tseng received the B.S. degree from National Taiwan University, Taipei, Taiwan, R.O.C., in 1986, and the M.S. and Ph.D. degrees from the University of California, Berkeley, in 1991 and 1994, respectively, all in mechanical engineering.

He is currently a Technical Leader at the Research and Innovation Center, Ford Motor Company, Dear-born, MI, where he has been since 1994. His previous work includes low pressure tire warning system using wheel speed sensors, traction control, electronic sta-bility control, and roll stability control. His current research interests include both powertrain and vehicle dynamics control.

Davor Hrovat (F'07) received the Dipl. Ing. degree from the University of Zagreb, Croatia, in 1972, and the M.S. and Ph.D. degrees in mechanical engi-neering from the University of California, Davis, in 1976 and 1979, respectifully.

Since 1981, he has been with the Ford Research Laboratory (FRL), Dearborn, MI, where he is a Henry Ford Technical Fellow coordinating and leading research efforts on various aspects of ve-hicle/power train control systems, where he holds numerous patents. He has served as an Associate Editor and as a member of the Board of Editors for a number of ASME, IEEE, IFAC, and other journals.

Dr. Hrovat was a recipient of the 1996 ASME/Dynamic Systems and Control Innovative Practice Award and the 1999 AACC Control Engineering Practice Award. He was recently elected to the National Academy of Engineering.